g-Anisotropy of the S_2-State Manganese Cluster in Single Crystals of Cyanobacterial Photosystem II Studied by W-Band Electron Paramagnetic Resonance Spectroscopy

Hideto Matsuoka,[†,‡] Ko Furukawa,[†] Tatsuhisa Kato,*[,†,§] Hiroyuki Mino,[||] Jian-Ren Shen,[⊥] and Asako Kawamori*[,#,▽]

Institute for Molecular Science, Okazaki 444-8585, Japan, Department of Chemistry, Faculty of Science, Josai University, Sakado, Saitama 350-0295, Japan, Division of Material Science (Physics), Graduate School of Science, Nagoya University, Nagoya 464-8602, Japan, Department of Biology, Faculty of Science, Okayama University, Naka-Tsushima, Okayama 700-8530, Japan, Precursory Research for Embryonic Science and Technology (PRESTO), Japan Science and Technology Agency, Japan, and School of Science and Technology, Kwansei Gakuin University, Sanda, Hyogo 669-1337, Japan

Received: September 5, 2005; In Final Form: May 8, 2006

The multiline signal from the S_2-state manganese cluster in the oxygen evolving complex of photosystem II (PSII) was observed in single crystals of a thermophilic cyanobacterium *Thermosynechococcus vulcanus* for the first time by W-band (94 GHz) electron paramagnetic resonance (EPR). At W-band, spectra were characterized by the *g*-anisotropy, which enabled the precise determination of the tensor. Distinct hyperfine splittings (hfs's) as seen in frozen solutions of PSII at X-band (9.5 GHz) were detected in most of the crystal orientations relative to the magnetic field. In some orientations, however, the hfs's disappeared due to overlapping of a large number of EPR lines from eight crystallographic symmetry-related sites of the manganese cluster within the unit cell of the crystal. Analysis of the orientation-dependent spectral features yielded the following **g**-tensor components: $g_x = 1.988$, $g_y = 1.981$, $g_z = 1.965$. The principal values suggested an approximate axial symmetry around the Mn(III) ion in the cluster.

Introduction

Photosystem II (PSII) in plants and cyanobacteria catalyzes water oxidation using solar energy, feeding our biosphere with an unlimited amount of molecular oxygen. The water-oxidizing complex (WOC) of PSII consists of four exchange-coupled manganese (Mn) atoms, which undergo stepwise oxidation upon abstraction of electrons.[1,2] Kok et al. showed[3] that the WOC accumulates four positive charges to evolve one oxygen molecule. The intermediate oxidation states have been termed the S_i state with $i = 0-4$. The S_1 state is the thermodynamically most stable state, and the S_4 state is a transient state immediately followed by oxygen evolution and regeneration of the S_0 state.

Extended X-ray absorption fine structure (EXAFS) studies of the WOC have led to proposals for a number of model structures: a dimer of dimers including disproportional cubane-like structures[4−8] and a core of three strongly coupled Mn ions linked with a weakly coupled fourth Mn (the so-called 3 + 1 model).[9,10] In addition, very recently, the crystal structure of PSII was reported for two species of cyanobacteria, *Thermosynechococcus elongates*[11−13] and *Thermosynechococcus vulcanus*.[14] The space groups of all PSII crystals reported so far were $P2_12_12_1$, in which one unit cell is composed of four PSII complexes. Since the PSII complex was made up of a dimer in the crystal, as in the membranes, eight PSII monomers were included in one unit cell; consequently, there are eight sites of the Mn cluster in each unit cell. All of the crystal structures showed that the Mn cluster has a 3 + 1 structure with three closely located atoms and another rather separated one, although the position of each Mn atom differs slightly in the different structural studies.[11−14] The structure of PSII at 3.5 Å resolution from *T. elongatus* showed that the Mn cluster contained additionally a Ca atom positioned in a site close to the Mn trimer, demonstrating a structure of cubane-like Mn_3Ca center plus one Mn atom.[12] This is consistent with the close association of Ca with the Mn cluster as suggested from previous EXAFS studies.[15−17]

Electron paramagnetic resonance (EPR) spectroscopy has been one of the most powerful tools to examine electronic and molecular structures of the WOC. Dismukes and Siderer first reported a characteristic multiline EPR signal from the S_2 state at X-band (9.5 GHz),[18] which consisted of approximately 18 lines with an average spacing of 9 mT. Following the pioneering work, several research groups have observed the S_2-state multiline signal at different frequencies (3.5,[19] 9.5,[20−23] and 34 GHz[24,30,32]), which have led to a number of proposals for magnetic interactions within the Mn cluster and the valence of each Mn ion in terms of the spin-Hamiltonian parameters. In particular, recent electron nuclear double resonance (ENDOR) studies of the S_2-state Mn cluster at X-band have provided detailed information on the hyperfine coupling (hfc) parameters of each Mn ion and led to the proposal of a trimer−monomer structural model for the Mn cluster.[25] It should be noted that all of the measurements reported so far were performed on noncrystalline samples of PSII at lower frequencies than Q-band

* Authors to whom correspondence should be addressed. E-mail: rik@josai.ac.jp (T.K.); agape-kawa@nifty.com (A.K.).
† Institute for Molecular Science.
‡ Present address: Chemical Dynamics Laboratory, RIKEN, Wako 351-0198, Japan.
§ Josai University.
|| Nagoya University.
⊥ Okayama University and Japan Science and Technology Agency.
Kwansei Gakuin University.
▽ Present address: AGAPE-Kabutoyama Institute of Medicine, Kabutoyama-cho 53-4, Nishinomoya 662-0001, Japan.

10.1021/jp055008f CCC: $33.50
Published on Web 06/13/2006

(34 GHz) and ambiguity still remains in the spectral analyses due to the large number of adjustable parameters.

At higher frequencies (≥94 GHz), the resolution of the **g**-tensor components is elevated. Consequently, the **g**-tensor of the WOC should be determined precisely by EPR measurements using single crystals of PSII at W-band (94 GHz). In fact, a recent W-band EPR study on single crystals of *T. elongatus* has led to the precise determination of the **g**-tensor of the tyrosine radical $Y_D^\bullet$ as well as its orientation relative to the crystal axes.[26] The present work demonstrates significant progress in EPR experiments on the WOC, i.e., the first detection of single-crystal W-band EPR spectra from the S_2-state Mn cluster. A part of the results has been reported in a preliminary form.[27]

Experimental Method

Sample Preparation. Cells of the thermophilic cyanobacterium *T. vulcanus* were grown, and the core particles of PSII were isolated as described previously.[28] Single crystals were grown as described before.[29] Well-defined crystals with an approximate size of $0.4 \times 0.2 \times 0.6$ mm^3 were inserted into quartz capillaries of an outer diameter of 0.9 mm.

Electron Paramagnetic Resonance Spectroscopy. The W-band EPR measurement was performed using a Bruker E680 spectrometer, with the temperature of the sample cavity controlled by a helium flow cryostat (Oxford Instruments model CF935) and a temperature controller (Oxford Instruments model ITC500).

To determine the orientation of the crystallographic axes with respect to the magnetic field, orientation-dependent W-band EPR spectra of the tyrosine radical $Y_D^\bullet$ were observed for dark-adapted crystal samples at 80 K. After that, to generate the S_2 state, the crystals were illuminated for 1 min at 200 K in the cavity with continuous light from a 100 W tungsten halogen lamp guided by an optical fiber. The crystals were cooled rapidly under illumination to trap the S_2 state, and the light was turned off at 160 K (this process took approximately 2 min). The temperature was further decreased to 6 K, where W-band measurements were performed. The orientation-dependent spectra were recorded every 15° by rotating the single-crystal samples about the capillary axis perpendicular to the magnetic field. EPR measurements in two planes of rotation were attained by using two single crystals with different orientations relative to the capillary axis.

Electron Paramagnetic Resonance Spectral Simulation. Computer simulation of EPR spectra was carried out by a modified program based on second-order perturbation theory, which was constructed using MATLAB 6.5 provided by MathWorks, Inc.[34] In the program, resonance fields and transition intensities were calculated with analytical expressions derived by Iwasaki.[33]

Results and Discussion

S_2-State Multiline Signal in Single Crystals and Frozen Solutions of PSII. Figure 1a shows the well-known multiline signal observed at X-band for the S_2 state in a frozen solution of PSII from *T. vulcanus*. In this work, the typical multiline signal was detected in single crystals of PSII from *T. vulcanus* at W-band, as shown in Figure 1c. However, as shown in Figure 1S of the Supporting Information, no distinct hyperfine splitting (hfs) was observed in the frozen solution at W-band due to the so-called *g*-strain effect, which originates in the distribution of *g*-factors related to variations among paramagnetic sites (Supporting Information). Therefore, it was demonstrated that W-band measurements of single crystals were crucial to improve the resolution of the *g*-anisotropy.

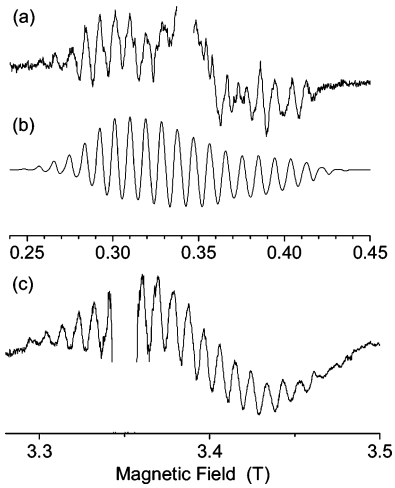

Figure 1. (a) Observed and (b) calculated X-band EPR spectra of the S_2 state in a frozen solution of PSII from *T. vulcanus*. For clarity, the $Y_D^\bullet$ signal at $g \approx 2$ is removed. The hf lines around 0.37 T in part a are disturbed by the EPR signal of the Q_A^- semiquinone radical anion. The spectral simulation was performed by using the following parameters: **g**-tensor in Table 1, **A**-tensors in ref 26, and a line width of 3.6 mT (full width at half-height, fwhh). (c) Light-minus-dark W-band spectrum of the S_2 state in single crystals of PSII from *T. vulcanus*. Experimental conditions: (a) microwave frequency 9.6 GHz, power 200 μW, temperature 6 K, time constant 82 ms, field sweep 0.025 T/min, modulation frequency 100 kHz, and amplitude 1 mT; (c) see the caption of Figure 2a.

Angular Variation of W-Band Spectra of the S_2-State Mn Cluster. Orientation-dependent EPR spectra of the S_2 state were observed at W-band by rotating a single crystal every 15° approximately about the crystallographic *a*-axis. The experimental spectra are depicted every 30° as black lines in Figure 2a, because inclusion of the whole spectra would make the hf structures unclear. The spectra were obtained by subtraction of the signal before the light illumination as abbreviated light-minus-dark spectra in Figure 2a. Since the subtraction procedure results in no significant correction for spectral analysis as described below, angular variations observed in the other crystal orientation will be shown without subtraction. In some specific crystal orientations, the hfs of the multiline signal consists of a maximum of 21 hf lines with an approximate spacing of 9 mT, which would be expected from four equivalently coupled Mn atoms. However, a close inspection indicated that the hf components are not equally spaced and that the separations between neighboring components depend on the crystal orientation with respect to the magnetic field. Thus, a symmetric cubic structure of the tetra-manganese center is apparently not applicable to illustrate these orientation-dependent hfs features.

Orientation-dependent spectra were also observed by rotating another single crystal every 15° about an arbitrary axis. The experimental spectra are depicted every 30° as black lines in Figure 3a. Because there was no significant improvement by the subtraction as mentioned above, only the spectra taken after illumination are shown in the figure. Residual background signals from the cavity contaminated by Mn^{2+}, which are marked by asterisks in the spectrum at 60°, are seen as six lines around the $Y_D^\bullet$ signal at 3.35 T. It should be noted that the distinctly resolved hfs are obscured at the setting of 60° where only the residual background signals are visible. The unmanipulated spectra in the figure ensure that the disappearance of the structure is not due to an accidental cancellation by the subtraction process. A nonequivalent tetranuclear manganese

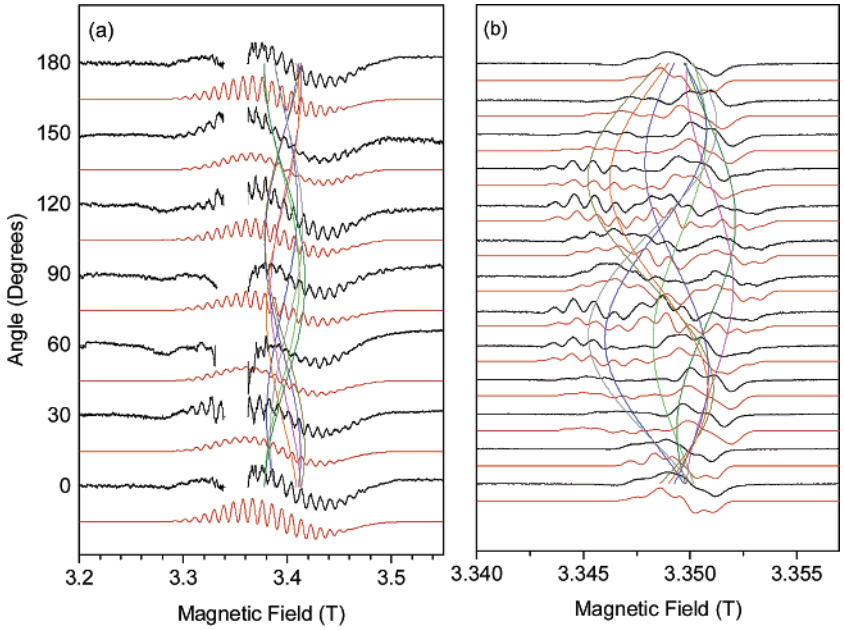

Figure 2. (a) Light-minus-dark W-band EPR spectra of the S_2 state in single crystals of PSII from *T. vulcanus*, which are depicted every 30°. For clarity, the $Y_D^\bullet$ signal at $g \approx 2$ is removed. The spectra were observed every 15° as a crystal was rotated approximately about the crystallographic *a*-axis. (b) Orientation-dependent W-band EPR spectra of the $Y_D^\bullet$ radical. The spectra were recorded in the same orientation as in part a. Black and red lines represent the experimental spectra and the best-fit simulation, respectively. The spectral simulation was performed by using the following parameters: (a) **g**-tensor in Table 1, **A**-tensors in ref 25, and a line width of 7.2 mT (fwhh); (b) **g**- and **A**-tensors in ref 26 and a line width of 0.72 mT (fwhh). Colored lines in parts a and b, which connect spectra measured at different orientations, show the angular variation of the effective *g*-values calculated for the eight crystallographic sites of the Mn cluster and $Y_D^\bullet$ radical, respectively. Experimental conditions: (a) microwave frequency 94.0 GHz, power 5 μW, temperature 6 K, time constant 82 ms, field sweep 0.025 T/min, modulation frequency 10 kHz, and amplitude 2 mT; (b) microwave frequency 94.0 GHz, power 50 nW, temperature 80 K, time constant 10 ms, modulation frequency 10 kHz, and amplitude 0.4 mT.

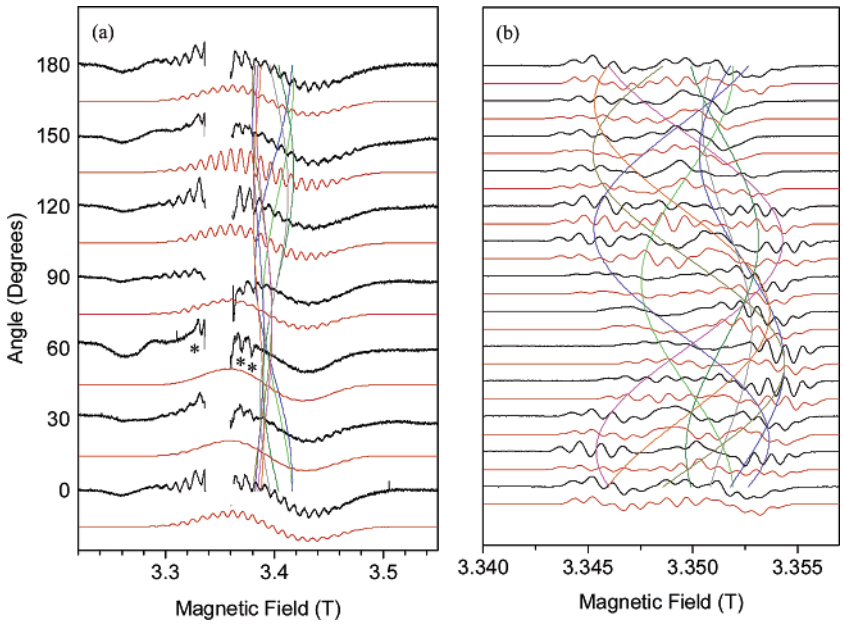

Figure 3. (a) S_2-state W-band spectra observed at a different crystal orientation from that in Figure 2a, which are depicted every 30°. For clarity, the $Y_D^\bullet$ signal at $g \approx 2$ is removed. Background signals from the cavity, which are marked by asterisks in the spectrum at 60°, overlap with the multiline signal around the $Y_D^\bullet$ signal. (b) Orientation-dependent W-band EPR spectra of the $Y_D^\bullet$ radical. The spectra were recorded in the same orientation as in part a. Black and red lines represent the experimental spectra and the best-fit simulation, respectively. Colored lines connecting different spectra in parts a and b show the angular variation of the effective *g*-values calculated for the eight crystallographic sites of the Mn cluster and $Y_D^\bullet$ radical, respectively. Experimental conditions and the spin-Hamiltonian parameters used here are the same as those in Figure 2.

cluster composed of four $I = {}^5/_2$ nuclei gives rise to a total of 1296 hf lines. In addition, since the crystal contains eight PSII complexes in one unit cell, the observed spectra include all contributions from the eight crystallographic sites of the Mn cluster. As shown below, the poor resolution of the hfs was caused by the overlapping of a large number of EPR lines, indicating that the appropriate crystal orientation with respect to the magnetic field is crucial to obtain the well-resolved multiline signal.

Determination of the Crystal Orientation Relative to the Magnetic Field. To determine the crystal orientation relative to the magnetic field, orientation-dependent spectra of $Y_D^\bullet$ were

TABLE 1: Principal Values and Orientations of the g-Tensor for One Dimer of the Eight Crystallographic Mn Sites Determined by the Spectral Analyses of the W-Band Spectra in Figures 2a and 3a[a]

	g_1			g_2			
	x_1	y_1	z_1	x_2	y_2	z_2	C_2
a	−0.0045	−0.9503	0.3113	0.5180	0.7460	−0.4186	0.282
b	0.8029	0.1821	0.5676	0.2143	−0.5869	−0.7807	0.558
c	−0.5961	0.2525	0.7622	−0.8281	0.3147	−0.4639	−0.781

[a] The direction of C_2 axis is given from ref 26: $g_x = 1.988$, $g_y = 1.981$, $g_z = 1.965$.

recorded at W-band. As shown in Figures 2b and 3b, the observed spectra were well reproduced by spectral simulation with the spin-Hamiltonian parameters reported by Hofbauer et al.[26] Colored lines in Figures 2b and 3b show the angular dependences of the effective *g*-values calculated for the eight symmetric sites. In Figure 2, the rotation axis of the magnetic field was approximately parallel to the *a*-axis. The crystallographic *b*- and *c*-axes were approximately parallel to the direction of the magnetic field at the settings of 0° and 90°, respectively. However, in Figure 3 the rotation axis was inclined from the *a*-axis by 78°, from the *b*-axis by 41°, and from the *c*-axis by 51°. Concerning the settings of 60° and 150° in the figure, the magnetic field direction is approximately parallel to the *a*-axis and to an axis along the *b*−*c* plane, respectively.

Determination of the *g*-Anisotropy. The angular dependence of the multiline spectra can be analyzed using the effective spin Hamiltonian given by

$$\hat{H} = \beta H \cdot \mathbf{g} \cdot S + \sum_i I_i \cdot \mathbf{A}_i \cdot S$$

where $S = {}^1/_2$ is the total spin resulting from exchange interactions between four Mn atoms, I_i is the nuclear spin of the *i*th manganese nuclei, and the summation is carried out over four manganese nuclei. An effective hf tensor $\mathbf{A}_i$ can be derived from the intrinsic hf tensors of the uncoupled Mn ions by using a projection matrix.[25] The nuclear quadrupole interaction may be neglected because of its small effect at high magnetic field.

Due to the overlapping of a large number of EPR lines, the effective *g*-values of the eight sites are difficult to trace in the experimental spectra. Therefore, the principal values and orientation of the **g**-tensor were determined by performing spectral simulation at every possible orientation of the tensor, where the principal values were also varied within the range of $1.96 \le g_x, g_y, g_z \le 2.00$ allowable from the frozen-solution X-band spectrum (Supporting Information). In the spectral simulation, we used the effective ^{55}Mn hfc constants estimated by Peloquin et al. from X-band ENDOR measurements on the S_2 state in a frozen solution of spinach PSII,[25] which are the most reliable parameters at present. The principal values of the hfc tensors were well explained by assuming a trimer−monomer structural model for the S_2 state.[25]

Red lines in Figures 2a and 3a show the best-fit simulation of the experimental spectra. The simulated spectra were obtained by summation of the spectra over the eight crystallographic sites of the cluster, whose relative orientations were determined by the symmetry operation of the crystallographic $P2_12_12_1$ space group. The orientation of the dimer axis determined by Hofbauer et al.[26] was employed in the simulation. Colored lines in Figures 2a and 3a show the angular dependences of the effective *g*-values calculated for the eight symmetric sites. Table 1 shows the principal values and orientations of the **g**-tensor determined for one dimer of the eight crystallographic Mn sites, where the g_x-, g_y-, and g_z-directions are given as direction cosines relative to the crystallographic axes (Supporting Information). Those of the tensor for the other sites can be obtained by considering the symmetry operation. Here, the direction of g_x is identical to that of A_z' defined in ref 25. The calculated spectra in Figure 2a show distinct peaks for all field orientations, whereas in Figure 3a the resolved hfs is obscured for some crystal orientations. These features fit well with the experimental spectra shown by black lines in the figures. The spectral simulation also reproduced the broad "background-like" signals arising from the S_2 state. Moreover, the simulation using the same parameters yielded a spectrum that was in good agreement with the X-band spectra observed in frozen PSII solution as shown in Figure 1b.

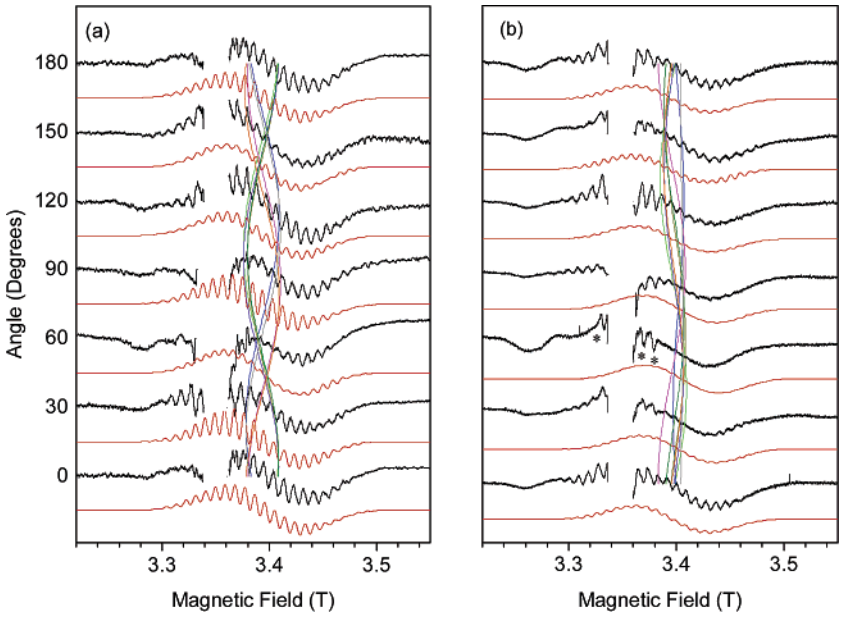

Figure 4. Observed and calculated S_2-state W-band spectra shown by black and red lines, respectively. The experimental spectra in parts a and b correspond to those in Figures 2a and 3a, respectively. The spectral simulation was performed by using the following parameters: **g**-tensor in Table 2, **A**-tensors in ref 25, and a line width of 7.2 mT (fwhh).

TABLE 2: Principal Values and Orientations of the g-Tensor Used in Figure 4[a]

	g_1			g_2			
	x_1	y_1	z_1	x_2	y_2	z_2	C_2
a	0.9847	−0.1567	0.0763	0.2515	−0.2726	−0.9287	0.282
b	−0.0445	−0.6493	−0.7592	0.9274	0.3424	0.1506	0.558
c	0.1686	0.7442	−0.6463	0.2769	−0.8992	0.3389	−0.781

[a] These values were obtained by employing the tensor in ref 25 as the initial parameter of the least-squares fitting procedure: $g_x = 1.989$, $g_y = 1.972$, $g_z = 1.970$.

It should be noted that there is a remarkable difference between the **g**-tensors determined in this work and those in ref 25. We also evaluated the **g**-tensor by spectral simulation with the help of a least-squares fitting procedure described previously,[34] where the **g**-tensor in ref 25 was employed as the initial parameter of the fitting procedure. Figures 4a and 4b show the best-fit simulation obtained from the spectral analysis. The **g**-tensor used in the simulation was given in Table 2. The direction of g_x is again identical to that of A_z' defined in ref 25. The spectral simulation reproduced the positions of the distinct hf lines and their disappearance. However, the broad background-like signals could not be completely reproduced. Therefore, it is concluded that the **g**-tensor given in Table 1 is more reliable.

On closer inspection of Figures 2a and 3a, differences in the positions and separations of the hf lines were found between the observed and simulated spectra in several orientations of the single crystals. The deviation may be ascribed not only to inaccuracy of the angle settings but also to the assumptions that the four **A**-tensors have axial symmetry and the same orientation as the effective **g**-tensor. W-band pulsed-ENDOR experiments on the PSII crystal would improve the disagreement.

Relationship between *g*-Anisotropy and Geometrical Structure of the Mn Cluster. Figure 5a shows the C_2 dimer axis and geometrical structures of the Mn cluster proposed by the crystal structural analyses.[11,12,14] Here, the membrane normal is parallel to the C_2 axis. Figure 5b depicts the relative orientation of the two g_z-directions given by direction cosines in Table 1 and crystallographic axes with respect to the C_2 axis in Figure 5a. At present, the generally accepted oxidation state for the S_2 state is Mn(III, IV, IV, IV). The ground state of a Mn(III) ion with $3d^4$ configuration is ^5E_g in an octahedral field, and that of a Mn(IV) ion with $3d^3$ configuration is $^4A_{2g}$. Consequently, the *g*-anisotropy of a Mn(III) ion is usually larger compared to that of Mn(IV) with the isotropic electronic ground state. Therefore, as seen in other mixed valence systems of Mn(III)Mn(IV),[31] the *g*-anisotropy of the S_2 state is expected to be dominated by that of the Mn(III) ion in the cluster. In other words, the principal values of the effective **g**-tensor suggest that the Mn(III) ion occupies an axially symmetric site.

Under a tetragonal field, the ^5E_g ground state of the Mn(III) ion splits into $^5A_{1g}$ and $^5B_{1g}$, and the *g*-values are given by[35]

$$g_{||} = g_e - \frac{8\lambda}{\Delta E} \quad g_\perp = g_e - \frac{2\lambda}{\Delta E} \quad \text{for the } ^5B_{1g} \text{ ground state}$$

$$g_{||} = g_e \quad g_\perp = g_e - \frac{6\lambda}{\Delta E} \quad \text{for the } ^5A_{1g} \text{ ground state}$$

where g_e is the *g*-factor of the free electron, ΔE is the energy difference between the ground and the excited states, and λ is the spin−orbit coupling constant. As shown in Table 1, the *g*-anisotropy of the S_2 state can be interpreted well by assuming the $^5B_{1g}$ ground state. The result suggests that the g_z-direction in Figure 5 is parallel to the d_{z^2} direction of the Mn(III) ion in the Mn cluster and also to the tetragonally distorted axis.

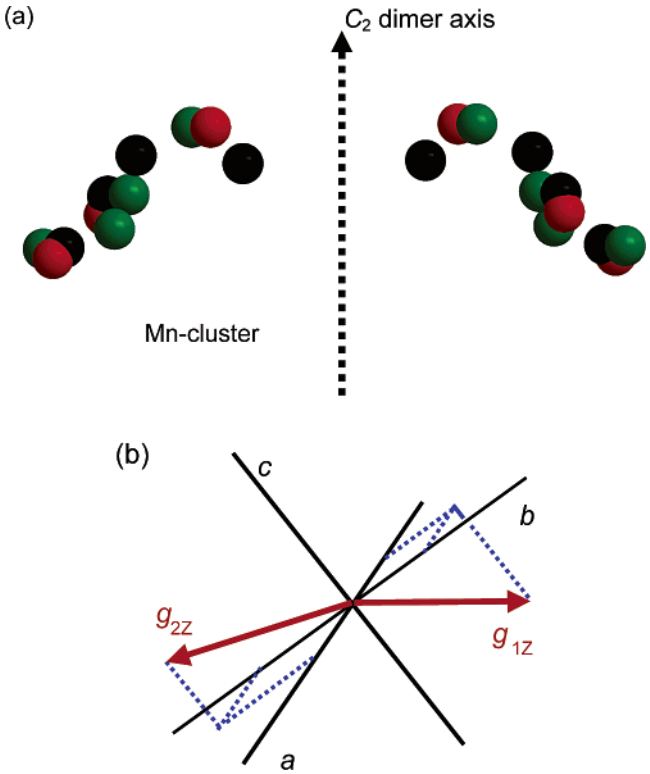

Figure 5. (a) Geometrical structures of the Mn cluster with respect to the C_2 dimer axis. Those of the Mn cluster depicted by green, black, and red circles are derived from the crystal structures in refs 11, 12, and 14, respectively. The orientation of the dimer axis was determined by W-band EPR spectroscopy.[26] (b) Relative orientation of the g_z-directions and crystallographic axes with respect to the dimer axis in part a. The two g_z-directions are defined by the direction cosines (0.3113, 0.5676, 0.7622) and (−0.4186, −0.7807, −0.4639) given in Table 1.

Conclusion

The use of PSII single crystals allowed the detection of an orientation-dependent S_2 multiline signal by W-band EPR for the first time and the precise determination of the *g*-anisotropy. The principal values of the **g**-tensor indicated that the Mn(III) ion in the cluster exists in an approximate axial symmetry. The single-crystal spectra were reasonably interpreted by spectral simulation with the hfc parameters appropriate for a trimer−monomer structure of the Mn cluster. This work demonstrated that single-crystal experiments are crucial to detect the characteristic and well-resolved hfs of the S_2 state at W-band. High-field ENDOR experiments on the PSII crystal are underway for a more detailed understanding of the mechanism of oxygen evolution.

Acknowledgment. The authors thank the Research Center for Molecular-Scale Nano-science, Institute for Molecular Science, for utilization of the W-band EPR spectrometer. We also thank Dr. Christopher W. M. Kay (Free University Berlin, Germany) for helpful discussions. H. Mino acknowledges the 21st Century COE program "The Origin of the Universe and Matter" of Nagoya University from the MECSST of Japan. H. Matsuoka acknowledges Research Fellowships of the Japan Society for the Promotion of Science for Young Scientists. This work was supported in part by Grants-in-Aid for Scientific Research from the Ministry of Education, Science and Culture of Japan.

Supporting Information Available: Description of the procedure for determining the **g**-tensor and spectral simulations of the single-crystal and frozen-solution spectra at X- and W-band using several different line widths. This material is available free of charge via the Internet at http://pubs.acs.org.

References and Notes

(1) Britt, R. D. In *Oxygenic Photosynthesis: The Light Reactions*; Ort, D., Yocum, C. F., Eds.; Advances in Photosynthesis 4; Kluwer Academic Publishers: Dordrecht, The Netherlands, 1996; pp 137−164.

(2) Ke, B. *Photosynthesis: Photobiochemistry and Photobiophysics*; Kluwer Academic Publishers: Dordrecht, The Netherlands, 2001; pp 199−418.

(3) Kok B.; Forbush, B.; McGloin, M. *Photochem. Photobiol.* **1970**, *11*, 457.

(4) Yachandra, V. K.; Derose, V. J.; Latimer, M., J.; Mukerji, I.; Sauer, K.; Klein, M. P. *Science* **1993**, *260*, 675.

(5) DeRose, V. J.; Mukerji, I.; Latimer, M. J.; Yachandra, V. K.; Sauer, K.; Klein, M. P. *J. Am. Chem. Soc.* **1994**, *116*, 5239.

(6) Yachandra, V. K.; Sauer, K.; Klein, M. P. *Chem. Rev.* **1996**, *96*, 2927.

(7) Dau, H.; Iuzzolino, L.; Dittmer, J. *Biochim. Biophys. Acta* **2001**, *1503*, 24.

(8) Chen, H.; Faller, J. W.; Crabtree, R. H.; Brudvig, G. W. *J. Am. Chem. Soc.* **2004**, *126*, 7345.

(9) Robblee, J. H.; Messinger, J.; Cinco, R. M.; McFarlane, K. L.; Fernandez, C.; Pizarro, S. A.; Sauer, K.; Yachandra, V. K. *J. Am. Chem. Soc.* **2002**, *124*, 7459.

(10) Cinco, R. M.; Robblee, J. H.; Messinger, J.; Fernandez, C.; Holman, K. L. M.; Sauer, K.; Yachandra, V. K. *Biochemistry* **2004**, *43*, 13271.

(11) Zouni, A.; Witt, H. T.; Kern, J.; Fromme, P.; Krauss, N.; Saenger, W.; Orth, P. *Nature* **2001**, *409*, 739.

(12) Ferreira, K. N.; Iverson, T. M.; Maghlaoui, K.; Barber, J.; Iwata, S. *Science* **2004**, *303*, 1831.

(13) Biesiadka, J.; Loll, B.; Kern, J.; Irrgang, K.-D.; Zouni, A. *Phys. Chem. Chem. Phys.* **2004**, *6*, 4733.

(14) Kamiya, N.; Shen, J.-R. *Proc. Natl. Acad. Sci. U.S.A.* **2003**, *100*, 98.

(15) Cinco, R. M.; Holman, K. L. M.; Robblee, J. H.; Yano, J.; Pizarro, S. A.; Bellacchio, E.; Sauer, K.; Yachandra, V. K. *Biochemistry* **2002**, *41*, 12928.

(16) Latimer, M. J.; Derose, V. J.; Mukerji, I.; Yachandra, V. K.; Sauer, K.; Klein, M. P. *Biochemistry* **1995**, *34*, 10898.

(17) Latimer, M. J.; Derose, V. J.; Yachandra, V. K.; Sauer, K.; Klein, M. P. *J. Phys. Chem. B* **1998**, *102*, 8257.

(18) Dismukes, G. C.; Siderer, Y. *Proc. Natl. Acad. Sci. U.S.A.* **1981**, *78*, 274.

(19) Haddy, A.; Aasa, R.; Andreasson, L. E. *Biochemistry* **1989**, *28*, 6954.

(20) Zheng, M.; Dismukes, G. C. *Inorg. Chem.* **1996**, *35*, 3307.

(21) Hasegawa, K.; Kusunoki, M.; Inoue, Y.; Ono, T. A. *Biochemistry* **1998**, *37*, 9457.

(22) Lakshmi, K. V.; Eaton, S. S., Eaton; G. R.; Brudvig, G. W. *Biochemistry* **1999**, *38*, 12758.

(23) Åhrling, K. A.; Smith, P. J.; Pace, R. J. *J. Am. Chem. Soc.* **1998**, *120*, 13202.

(24) Smith, P. J.; Åhrling, K. A.; Pace, R. J. *J. Chem. Soc., Faraday Trans.* **1993**, *89*, 2863.

(25) Peloquin, J. M.; Cambell, K. A.; Randall, D. W.; Evanchik, M. A.; Pecoraro, V. L.; Armstrong, W. H.; Britt, R. D. *J. Am. Chem. Soc.* **2000**, *122*, 10926.

(26) Hofbauer, W.; Zouni, A.; Bittl, R.; Kern, J.; Orth, P.; Lendzian, F.; Fromme, P.; Witt, H. T.; Lubitz, W. *Proc. Natl. Acad. Sci. U.S.A.* **2001**, *98*, 6623.

(27) Kawamori, A.; Shen, J.-R.; Mino, H.; Furukawa, K.; Matsuoka, H.; Kato, T. In *Photosynthesis: Fundamental Aspects to Global Perspectives*; van der Est, A., Bruce, D., Eds.; Alliance Communications Group: Lawrence, KS, 2005; pp 406−408.

(28) Shen, J. R.; Inoue, Y. *Biochemistry* **1993**, *32*, 1825.

(29) Shen, J. R.; Kamiya, N. *Biochemistry* **2000**, *39*, 14739.

(30) Kulik, L. V.; Epel, B.; Lubitz, W.; Messinger, J. *J. Am. Chem. Soc.* **2005**, *127*, 2392.

(31) Yano, J.; Sauer, K.; Girerd, J.-J.; Yachandra, V. K. *J. Am. Chem. Soc.* **2004**, *126*, 7486.

(32) Haddy, A.; Lakshmi, K. V.; Brudvig, G. W.; Frankz, H. A. *Biophys. J.* **2004**, *87*, 2885.

(33) Iwasaki, M. *J. Magn. Reson.* **1974**, *16*, 417.

(34) Matsuoka, H.; Furukawa, K.; Sato, K.; Shiomi, D.; Kojima, Y.; Hirotsu, K.; Furuno, N.; Kato, T.; Takui, T. *J. Phys. Chem. A* **2003**, *107*, 11539.

(35) Griffith, J. S. In *The Theory of Transition-Metal Ions*; Cambridge University Press: New York, 1961.